THE ASTROPHYSICAL JOURNAL, 503:L19–L22, 1998 August 10

DEEP *H*-BAND GALAXY COUNTS AND HALF-LIGHT RADII FROM *HUBBLE SPACE TELESCOPE*/NICMOS PARALLEL OBSERVATIONS

LIN YAN, PATRICK J. MCCARTHY, LISA J. STORRIE-LOMBARDI, AND RAY J. WEYMANN
The Observatories of the Carnegie Institution of Washington, 813 Santa Barbara Street, Pasadena, CA 91101-1292
Received 1998 March 23; accepted 1998 April 22; published 1998 July 17

ABSTRACT

We present deep galaxy counts and half-light radii from F160W ($\lambda_c = 1.6$ μm) images obtained with the Near-Infrared Camera and Multiobject Spectrograph on the *Hubble Space Telescope*. Nearly 9 arcmin^2 have been imaged with camera 3, with 3 σ depths ranging from $H = 24.3$ to 25.5 in a 0.″6 diameter aperture. The slope of the counts fainter than $H = 20$ is 0.31, and the integrated surface density to $H \leq 24.75$ is 4×10^5 galaxies deg^{-2}. The half-light radii of the galaxies decline steeply with apparent magnitude. At $H = 24$, we are limited by both the delivered FWHM and the detection threshold of the images.

Subject headings: cosmology: observations — galaxies: evolution — infrared: galaxies

1. INTRODUCTION

Galaxy counts as a function of apparent magnitude probe both the geometry of the universe and the dynamical and luminosity evolution of galaxies. Evolutionary effects dominate the departures of the counts from the Euclidean expectation. The relative importance of the two primary forms of evolution, density and luminosity evolution, can only be properly assessed with spectroscopic redshifts. The near-IR passbands, however, are better suited than visible colors to purely photometric surveys since they are less sensitive to star formation and extinction. The weak dependence of the *k*-correction on Hubble type (Poggianti 1997) and its slow change with redshift further enhance the value of observing at wavelengths beyond ~1 μm.

The deepest visible galaxy counts yield an integrated galaxy number density of 2×10^6 deg^{-2} to m(F814W) = 29 (Williams et al. 1996). The deepest *K*-band counts reach $K = 23.5$ with limited areal coverage (~2 arcmin^2) and have a slope of $d \log N/dm \sim 0.2$–0.3 for $K > 18$ (Gardner, Cowie, & Wainscoat 1993; Djorgovski et al. 1995; Moustakas et al. 1997). The Near-Infrared Camera and Multiobject Spectrograph (NICMOS; Thompson et al. 1998) on the *Hubble Space Telescope* (*HST*) offers a means to extend the existing near-IR galaxy counts to much fainter levels in the equivalent of the *H* and *J* passbands. Parallel observations, in particular, provide modest sky coverage for deep galaxy counts. At the depth of the deepest Keck/NIRC *K* (2.2 μm) counts, our areal coverage is presently ~9 arcmin^2 and will increase as subsequent parallel exposures are taken. Our deepest pointings presently cover an area comparable to the deepest NIRC images but are roughly 1 mag deeper.

This Letter and the independent work of Teplitz et al. (1998) present the first deep *H*-band galaxy counts with NICMOS. Our data reach $H \sim 24.8$ (50% completeness limit), deeper than all previously published near-infrared counts. The F110W (~*J*) data, future parallel imaging observations, and a more detailed treatment of the present data will be presented in a separate publication.

2. OBSERVATIONS AND DATA REDUCTION

The data were obtained with camera 3 of NICMOS operating in the parallel mode, beginning in 1997 November. The NICMOS internal pupil adjustment mirror was set near the end of its range, providing the best possible focus for camera 3. The point-spread function (PSF), measured from the stars in a selected globular cluster field, is slightly non-Gaussian but is well characterized by FWHM = 0.″25.

We obtained four images per orbit, two each with the F110W ($\lambda_c = 1.1$ μm) and F160W ($\lambda_c = 1.6$ μm) filters. The field offset mirror was used to dither between two fixed positions 1.″8 apart in a direction aligned with one axis of the detector. In addition, there were small interorbit dither moves executed for some of the pointings. The detector was read using the STEP64 MultiAccum sample sequence, with 13 or 18 samples, resulting in exposure times of 256 and 576 s, respectively. The projected size of a camera 3 pixel is 0.″204, giving a 52.″2 × 52.″2 field of view for each image. A small area is lost in the construction of the final mosaic image. We selected 12 fields with intermediate to high galactic latitudes for this study (see Table 1). The areal coverage of the present data set is 8.7 arcmin^2.

We used McLeod's (1998) NicRed v1.5 package to linearize and remove the cosmic rays from the MultiAccum images. Median images were derived from the 24 pointings, and these were used to remove the dark and sky signals. Even with the optimal dark subtraction, there remain considerable frame-to-frame variations in the quality of the final images. We did not estimate photometric error for each individual galaxy because of the frame-to-frame variation; however, as described below, our incompleteness simulation has taken into account this effect for the galaxy number counts. The individual linearized, dark-corrected, flat-fielded, and cosmic-ray–cleaned images were shifted, masked, and combined to produce final mosaic images. Before shifting, each image was 2 × 2 block-replicated, and only integer (0.″1) offsets were applied. In this way, we avoided any smoothing or interpolation of the data. The MultiAccum process is not 100% efficient in rejecting cosmic-ray events, and so we applied a 3 σ rejection when assembling the final mosaics.

2.1. *Galaxy Detection and Photometry*

We performed the object detection and photometry using SExtractor version 1.2b10b (Bertin & Arnouts 1996) and the photometric zero points provided by M. Rieke (private communication 1997) with an uncertainty of 0.05 mag. Each image was convolved with a Gaussian kernel with FWHM = 0.″3 for object detection, using a 2.0 σ detection threshold. Isophotal magnitudes were measured to the 1 σ isophot.

We define the total magnitude in a manner similar to those

TABLE 1
THE SELECTED FIELDS

Field	R.A. (J2000)	Decl. (J2000)	l (deg)	b (deg)	T(F160W) (s)	$\mu(1\ \sigma)$ (mag arcsec^{-2})	$m_{\rm lim}$ (50%)	$N_{\rm lim}$ (50%)
0240−0141	02 40 13	−01 41 27	173	−54	2816	24.8	23.8	62
0304−0015	03 04 38	−00 15 04	178	−48	2560	25.3	23.8	25
0457−0456	04 57 19	−04 56 51	204	−28	4480	25.7	24.3	42
0729+6915	07 29 57	69 15 02	146	29	5120	25.9	24.5	31
0744+3757	07 44 32	37 57 21	182	26	2048	25.1	23.5	49
1039+4144	10 39 37	41 44 54	176	59	5376	25.5	24.5	74
1120+1300	11 20 35	13 00 00	242	65	13824	26.0	24.8	137
1237+6215	12 37 33	62 15 27	126	55	4608	25.7	24.3	47
1604+4318	16 04 55	43 18 56	69	48	3840	25.6	24.0	53
1631+3001	16 31 39	30 01 23	50	42	3584	25.1	24.0	88
2220−2442	22 20 12	−24 42 00	28	−56	5120	25.9	24.5	71
2344−1524	23 44 00	−15 24 50	66	−70	3840	25.4	24.0	60

NOTE.—Units of right ascension are hours, minutes, and seconds, and units of declination are degrees, arcminutes, and arcseconds.

used by Smail et al. (1995) and Djorgovski et al. (1995). SExtractor calculates isophotal and aperture magnitudes for each galaxy, along with the isophotal area at a given threshold. We adopted an aperture diameter of 0.″6. For galaxies with isophotal diameters less than 0.″6, we use their aperture magnitudes, after correction to a 2″ diameter aperture. In using the aperture magnitude as a total magnitude, we assumed that all faint galaxies have similar profiles. We derived the aperture correction from an average of 20 galaxies with isophotal diameters smaller than 0.″6. This average faint galaxy yielded an aperture correction of 0.3 ± 0.05 mag, which is indistinguishable from that derived from stars with $H \sim 18$.

For galaxies with isophotal diameters between 0.″6 and 2″, we measure isophotal magnitudes to 1 σ of sky and then correct to a 2″ diameter aperture using a correction that is a function of the isophotal magnitude. In our deepest field, for $H < 22.5$, the magnitude correction is negligible; for $22.5 < H < 23.5$ and $H > 23.5$, the corrections are 0.1 and 0.2 mag, respectively. These corrections are derived for each field in the same fashion as the aperture correction described above. Using the galactic foreground extinction A_B derived from the Burstein & Heiles maps (Burstein & Heiles 1984) and the extinction law derived by Rieke & Lebofsky (1985), we find that the maximum extinction correction for our fields is $A_H \sim 0.03$ mag. The new dust maps by Schlegel, Finkeiner, & Davis (1997) give the maximum A_H of 0.05 mag. Thus, we did not apply any extinction correction to our photometry.

The sky variances, measured in 10 blank 2.″5 × 2.″5 areas in each image, give 1 σ surface brightness limits ranging from 24.8 to 26.0 mag arcsec^{-2}. This implies 3 σ limits within a 0.″3 radius aperture of 24.3–25.5 mag.

2.2. *Incompleteness Modeling*

The raw counts must be corrected for false detections and incompleteness due to crowding, flat-field and dark correction errors, and Poisson noise before meaningful conclusions can be drawn. We have carried out an extensive series of simulations to quantify the incompleteness effects. We selected several well-detected galaxies from an image, dimmed them by various factors, and added these images into the original image at *random locations*. We then apply the same detection and photometry algorithms as in the original analyses. The use of random positions in the simulation allows us to include completeness corrections arising from nondetections and magnitude errors caused by crowding and spatially dependent errors in the sky subtraction and flat-field correction. With this approach, we create a matrix, P_{ir}, which is the probability of finding a galaxy with the input magnitude of m_i and the recovered magnitude m_r. The number of input galaxies N_i at each magnitude m_i was chosen to reproduce an initial guess for the slope of the counts. The number of galaxies recovered at magnitude m_i, N_r, is obtained from $\sum_i P_{ir} N_i$. The detection rate r_i is N_r/N_i, and the completeness correction at the corresponding magnitude bin is $1/r_i$. For each image, we did more than 10^4 simulations to estimate the incompleteness corrections. We performed the incompleteness modeling for four fields with representative integration times. The correction was applied to the individual fields before the final galaxy number counts were produced.

Of our 12 fields, three are at intermediate galactic latitudes. In these fields, we identified stars using the SExtractor star/galaxy classifier. We found four stars with magnitudes $20 < H < 22$, which implies an average 2% correction to the number counts; for $H > 22.0$, the correction at each magnitude bin is less than 2%. At $H > 24$, the counts are dominated by compact galaxies in all of our fields. In addition, the measurements of half-light radii versus total magnitude suggest that the stellar contamination in all of our fields is on the order of a few percent.

We estimated our false positive detection rate by reducing the "left" and "right" dither positions independently and by splitting our longest pointing into three independent, but shallower, data sets. The left and right dither position images allowed us to assess the impact of persistent cosmic rays, while the photometric catalogs in the $\frac{1}{3}$ exposure time images of 1120 + 1300 allowed us to assess the number of detections that had no corresponding object in the deeper image. Both approaches yield false detection rates in a few percent range in the faintest magnitude bin for each field.

2.3. *Half-Light Radii*

We measured the half-light radius for each object in the final photometric catalog. A subsection of the image centered on each object was extracted and regridded with 20 times finer sampling. The enclosed flux was then computed in 0.″005 steps (1/20 pixel) until one-half of the total flux was enclosed. The code used for this operation was kindly provided by I. Smail, and so our results can be compared directly with those of Smail et al. (1995). We measured the half-light radii of stars with $16 < H < 23$ in one globular cluster field to derive the instrumental half-light radius. The non-Gaussian shape of the PSF requires this measurement in order to allow a comparison with the derived galaxy sizes.

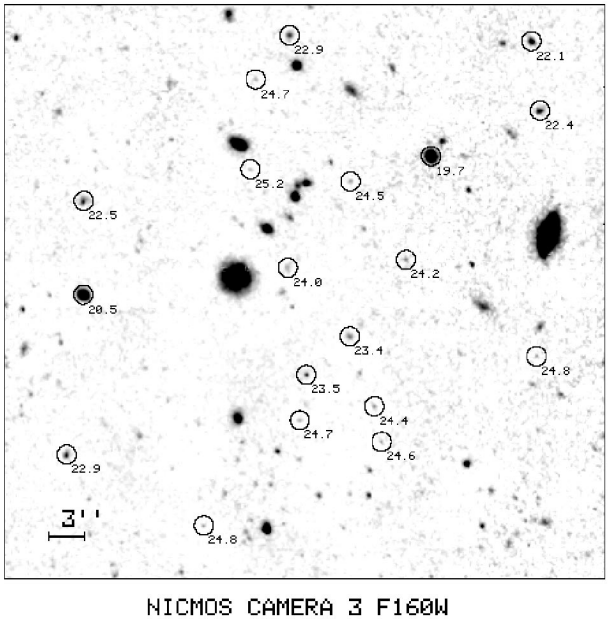

FIG. 1.—A gray-scale representation of our deepest field, 1121 + 1300. Several faint objects are marked, and their *H* magnitudes are noted. The field shown is 50.″2 × 50.″2.

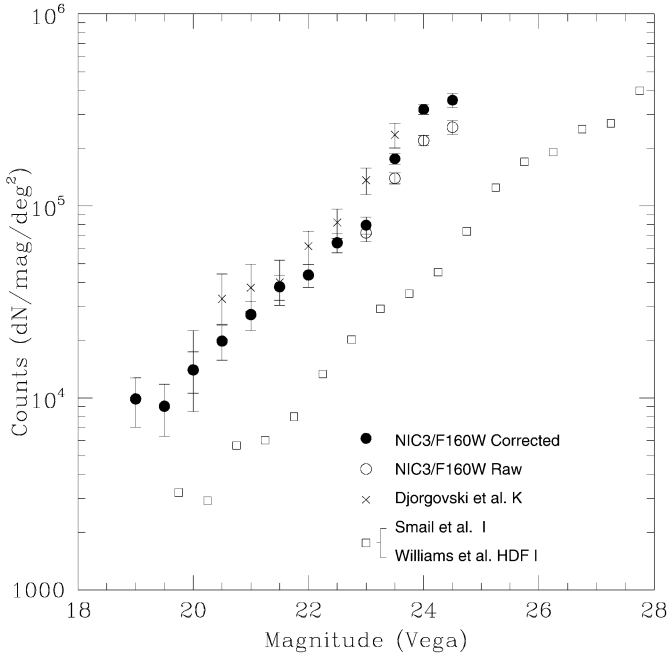

FIG. 2.—The galaxy number count–magnitude relation derived from our data and other surveys from the literature. The open and filled circles are the raw and corrected NICMOS *H* counts, respectively. The crosses are Djorgovski et al.'s (1995) *K* (2.2 μm) counts; the open squares are the average of the *I*-band counts from Smail et al. (1995) and Williams et al. (1996), with a zero-point shift of 0.48 mag applied to the AB magnitudes in Williams et al. to bring them to the system used in Smail et al.

2.4. *Results and Discussion*

Our deepest field, 1120 + 1300, is shown in Figure 1. We have circled several representative faint galaxies and noted their magnitudes. The two brightest galaxies in this field have isophotal magnitudes of 17.6 and 18.8, respectively. In Figure 2, we plot the raw and corrected differential galaxy number counts. Table 2 lists the raw counts, incompleteness-corrected counts, and effective area at each magnitude bin. We determine a slope of 0.31 ± 0.02 for $20 < H < 24.5$, which is consistent with the values derived at *K* by various groups (Gardner et al. 1993; Djorgovski et al. 1995; Moustakas et al. 1997). We find no significant change in the slope for $H < 24.5$. In the same figure, we plot the counts measured in *I* and *K* passbands by Smail et al. (1995), Williams et al. (1996), and Djorgovski et al. (1995). The integrated number of galaxies $H \leq 24.5$, including the incompleteness corrections, is 4×10^5 deg^{-2}, or 2×10^{10} galaxies over the entire sky. This is about 3 times larger than the total implied from the integration of the local luminosity function (Lin et al. 1996) to $0.01L^*$ over an all-sky comoving volume for the $(\Omega_0, \Omega_\Lambda) = (1, 0)$ cosmological model.

The unambiguous interpretation of the measured counts-magnitude relation in the context of the galaxy formation and evolution requires knowledge of both the redshift distribution and the faint-end slope of the luminosity function. Our images probe the faint-end slope as well as the distant universe. At $z = 1$, $H = 24$ corresponds to a luminosity of $\sim 0.01L^*$ ($H_0 = 50$ km s^{-1} Mpc^{-1}, $q_0 = 0.1$, $M_K^* = -24.75$ [Gardner et al. 1997; Glazebrook et al. 1995]). The *K*-band–selected spectroscopic surveys of Cowie et al. (1996, 1998) reach a median *z* of unity at $K = 20$–21.5, equivalent to $H \sim 21$–22.5 for mild to passively evolving populations at $z \sim 1$. Thus, our deep counts must contain a large number of $z > 1$ galaxies. The Lyman break–selected galaxies with spectroscopic redshifts also have *K*-band magnitudes of ~21.5–23 (Steidel et al. 1996), within the depths of the counts presented here. What is unclear at present is whether the median redshift continues to climb at faint *H* and *K* magnitudes or whether low-luminosity galaxies make an increasing contribution to the counts at $H > 23$. This could be clarified by the photometric redshift measurements of these faint galaxies. The shallow and deep *K*-band surveys by Huang et al. (1997) and Cowie et al. (1996, 1998) find $B - K$ colors that become increasingly blue for galaxies with $K > 18$, suggesting an increasing contribution from star-forming systems. If the bulk of the galaxies that we detect at $H \sim 24$ are faint dwarf galaxies with luminosity much less than L^* at low redshifts instead of L^* galaxies at $z > 3$, the counts' slope of 0.31 implies a luminosity function $\Phi(L) \propto L^{-1.78}$, which is steeper than the local luminosity function. Although there is some evidence that the faint end of the local luminosity function may be steeper than the standard value of −1 (Lilly et al. 1995), a slope of −1.78 has not been observed.

TABLE 2

RAW AND CORRECTED COUNTS

Magnitude	log N_{raw} (deg^{-2} mag^{-1})	log N_{corr} (deg^{-2} mag^{-1})	$-\sigma$	$+\sigma$	A_{eff} (arcmin^2)
19.0	3.995	3.995	0.148	0.11	8.7
19.5	3.957	3.957	0.156	0.114	8.7
20.0	4.146	4.146	0.121	0.094	8.7
20.5	4.296	4.296	0.099	0.081	8.7
21.0	4.434	4.434	0.083	0.070	8.7
21.5	4.579	4.579	0.069	0.0597	8.7
22.0	4.640	4.640	0.064	0.056	8.7
22.5	4.808	4.808	0.052	0.0466	8.7
23.0	4.860	4.900	0.047	0.042	8.7
23.5	5.144	5.267	0.028	0.028	8.7
24.0	5.340	5.503	0.026	0.026	6.5
24.5	5.410	5.551	0.038	0.035	2.9

NOTE.—Errors are in logarithmic scale, and A_{eff} is the effective area at each magnitude bin.

In Figure 3, we plot the measured half-light radii for all of the galaxies in our photometric catalog against their total magnitudes. We computed the median sizes in bins of 0.5 or 1 mag widths with the error bars as $\pm 1\ \sigma$ of the mean, and these are shown as the solid symbols in Figure 3. The dotted line corresponds to a uniform surface brightness of 22 mag arcsec^{-2}. It is clear from the crowding of points at the faint end into the small area between the stellar locus and the surface brightness limit that there are strong surface brightness selection effects in our sample at the faint end. Resolved objects with magnitudes fainter than $H \sim 24$ are undetectable in our data. For $H < 22$–23, however, there appears to be a real deficit of galaxies near our surface brightness limit, suggesting that the decrease in median half-light radius in the range $20 < H < 23$ is genuine. Images obtained with the high-resolution cameras on NICMOS will allow one to extend the study of galaxy scale lengths to scales of $\lesssim 0\farcs1$, but the surface brightness selection biases, on average, will be more severe for those data.

The NICMOS pure parallel program offers us a wealth of unique data with high angular resolution and unprecedented photometric depth in the H and J bands over an area of ~100 arcmin^2. We will be able to carry out much more detailed studies, such as deep number counts as functions of morphological types and colors and the evolution of galaxy intrinsic sizes. Combined with ground-based optical photometry and spectroscopy, we may be able derive photometric redshifts for the numerous faint galaxies detected in the galaxy number counts.

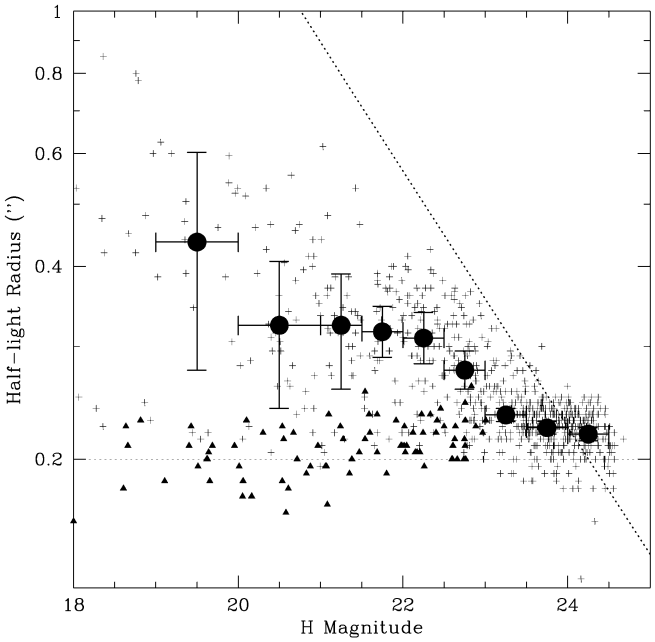

FIG. 3.—The half-light radii for all of the detected galaxies. Stellar objects are indicated by star symbols and galaxies by open circles. The filled circles indicate the median sizes in bins of 0.5 or 1 mag widths. At $H = 24$, we have reached the NIC3 angular resolution limit, $0\farcs2$. The diagonal dotted line shows the magnitude enclosed in an aperture of radius r with a uniform surface brightness of 22 mag arcsec^{-2}.

We thank the staff of the Space Telescope Science Institute for their efforts in making this parallel program possible. In particular, we thank Peg Stanley and the staff of the PRESTO division, Bill Sparks, John Mackenty, and Daniella Calzetti of the NICMOS group, and Bob Williams and Duccio Macchetto of the director's office. We acknowledge useful discussions with D. Hogg, I. Smail, R. Thompson, and M. Rieke. B. McLeod and I. Smail are thanked for generously allowing the use of their software for the data reduction and scale length measurements. This research was supported, in part, by grants from the Space Telescope Science Institute, GO-7498.01-96A and P423101. This project made use of the NASA/IPAC Extragalactic Database, operated by the Jet Propulsion Laboratory, California Institute of Technology, under contract with the National Aeronautics and Space Administration.

REFERENCES

Bertin, E., & Arnouts, S. 1996, A&AS, 117, 393
Burstein, D., & Heiles, C. 1984, ApJS, 54, 33
Cowie, L. L., et al. 1998, in preparation
Cowie, L. L., Songalia, A., Hu, E. M., & Cohen, J. G. 1996, AJ, 112, 839
Djorgovski, S., et al. 1995, ApJ, 438, L13
Gardner, J. P., Cowie, L. L., & Wainscoat, R. J. 1993, ApJ, 415, 9
Gardner, J. P., Sharples, R. M., Frenk, C. S., Baugh, C. M., & Carrasco, B. E. 1997, ApJ, 480, L99
Glazebrook, K., Peacock, J. A., Miller, L., & Collins, C. A. 1995, MNRAS, 275, 169
Huang, J. S., Cowie, L. L., Gardner, J. P., Hu, E. M., Songaila, A., & Wainscoat, R. J. 1997, ApJ, 476, 12
Lilly, S. J., Tresse, L., Hammer, F., Le Fevre, O., & Crampton, D. 1995, ApJ, 455, 108
Lin, H., Kirshner, R. P., Shectman, S. A., Landy, S. D., Oemler, A., Tucker, D. L., & Schecter, P. L. 1996, ApJ, 464, 60
McLeod, B. 1998, in the 1997 *HST* Calibration Workshop, ed. S. Casertano (Baltimore: STScI), in press
Moustakas, L. A., Davis, M., Graham, J. R., Silk, J., Peterson, B., & Yoshii, Y. 1997, ApJ, 475, 445
Poggianti, B. M. 1997, A&AS, 122, 399
Rieke, G., & Lebofsky, M. J. 1985, ApJ, 288, 618
Schlegel, D.J., Finkbeiner, D.P., & Davis, M. 1998, ApJ 500, 525
Smail, I., Hogg, D. W., Yan, L., & Cohen, J. G. 1995, ApJ, 449, L105
Steidel, C. C., Giavalisco, M., Pettini, M., Dickinson, M., & Adelberger, K. 1996, ApJ, 462, L17
Teplitz, H. I., et al. 1998, in preparation
Thompson, R. I., Rieke, M., Schneider, G., Hines, D., & Corbin, M. 1998, ApJ, 492, L95
Williams, R. E., et al. 1996, AJ, 112, 1335